Nonaxisymmetric thermal equilibria of a cylindrically bounded guiding-center plasma or discrete vortex system

Ralph A. Smith and Thomas M. O'Neil
Department of Physics, B-019, University of California, San Diego, La Jolla, California 92093

(Received 26 March 1990; accepted 16 July 1990)

The thermal equilibria of a two-dimensional guiding-center model for a single-species plasma bounded by a cylindrical conductor are considered in the microcanonical ensemble. The same description applies to identical point vortices in a two-dimensional, ideal fluid surrounded by a circular streamline. The statistically dominant configurations are displaced asymmetrically from the axis, for sufficiently large energies at specified canonical angular momentum. The transition between symmetric and asymmetric states resembles a second-order phase transition, and occurs at negative temperatures. It is related to a bifurcation in the mean-field (Vlasov) description. The theory is compared with Monte Carlo simulations of microcanonical ensembles of guiding centers.

I. INTRODUCTION

In this paper, we demonstrate that thermal equilibrium states of a cylindrically bounded, single-species, two-dimensional (2-D) guiding-center plasma or point-vortex gas are displaced from the center of the system for certain values of the constants of the motion. That is, the statistically predominant configurations of such a system do not have the rotational symmetry of the underlying confinement geometry at sufficiently large energies. The broken symmetry may be interpreted as the spontaneous excitation of a finite amplitude diocotron mode. Such equilibria have formally negative temperatures, and may describe non-neutral plasma columns in cylindrical Penning traps on intermediate time scales. Some of the work discussed below was summarized in an earlier letter.[1]

The system under consideration is a collection of N identical long rods of length L and charge q. (The point-vortex analogy will be defined below.) The rods are parallel to a uniform magnetic field $B\hat{z}$ and surrounded by a grounded conducting cylinder at radius $r = R$. We use cylindrical polar coordinates (r,θ,z) throughout. When not otherwise qualified, the term *symmetric* will subsequently mean "independent of the azimuthal angle θ." Each rod moves with the drift velocity $\mathbf{v} = (c/B)\mathbf{E}\times\hat{z}$ due to the electrostatic field $\mathbf{E}$ determined by the rod positions and the conducting boundary. For simplicity, we assume that L is sufficiently large that finite-length corrections to the electric field may be neglected. We regard this system as a 2-D guiding-center model of a magnetically confined, non-neutral plasma column.

We study microcanonical ensembles of guiding-center systems using two approaches. Most of the discussion is based on a Vlasov or mean-field description, where many analytical results are available. We also employ a Monte Carlo scheme to simulate the ensemble directly; this confirms some of the predictions of mean-field theory, and shows when correlation effects may be important.

In the mean-field description, a configuration of the system is specified by a continuous charge density $qn(r,\theta)$. Associated with this density is a self-consistent electrostatic potential ϕ satisfying Poisson's equation, $\nabla^2\phi = -4\pi qn$, subject to the boundary condition that $\phi = 0$ at the boundary $r = R$. (Sometimes we will write the inverse relation as $\phi = -4\pi q\nabla^{-2}n$.) The mean-field approximation applies when N is sufficiently large and certain correlations are weak; we will return to this point later.

The number of rods is related to the density through $N = L\int d^2\mathbf{r}\, n$, where $d^2\mathbf{r} = r\,dr\,d\theta$. The total energy is given by $E = (qL/2)\int d^2\mathbf{r}\, n\phi$ and the total canonical angular momentum by

$$M = \left(\frac{qL}{c}\right)\int d^2\mathbf{r}\, nrA_\theta(r) = \left(\frac{qBL}{2c}\right)\int d^2\mathbf{r}\, r^2 n,$$

where $A_\theta = Br/2$ is the vector potential for the uniform axial magnetic field. Inertia is neglected in the 2-D guiding center model, so the energy is entirely electrostatic, and the canonical angular momentum consists solely of the vector potential contribution. The confinement geometry is invariant under translations in time and azimuth, so E and M are conserved during evolution of the system, as is N.

The guiding-center plasma is dynamically equivalent to a collection of identical point vortices in a two-dimensional fluid surrounded by a circular streamline. Each vortex has circulation $4\pi qc/BL$, and is advected by the velocity field induced by the others. The mean-field vorticity is then $4\pi qcn/B$, and the streamfunction is $c\phi/B$. The statistics of this discrete system may describe some features of a turbulent two-dimensional fluid at large Reynolds numbers.[2] The remainder of our discussion will employ the language appropriate to the line-charge model.

Our goal is a statistical description of an isolated collection of guiding centers. Such a description is provided by averages over Gibbs's microcanonical ensemble, which is the set of all configurations having specified values of N, E, and M. For sufficiently large N, the entropy functional $S = -L\int d^2\mathbf{r}\, n\ln n$ gives a logarithmic measure of the number of microscopic configurations corresponding to a

 0899-8221/90/122961-15$02.00

macroscopic distribution $n(r,\theta)$. The most probable density distribution is found in the usual manner by maximizing S subject to the fixed values of N, E, and M. We will refer to these maximum entropy solutions as thermal equilibria. From the variational equation

$$\delta S - \beta(\delta E + \omega \delta M) - \gamma \delta N = 0, \tag{1}$$

where β, $\beta\omega$, and γ are Lagrange multipliers, one easily sees that S is an extremum for distributions of the form

$$n = n_0 \exp\{-\beta[q\phi + \omega(eB/2c)r^2]\}. \tag{2}$$

Here, ϕ must be determined self-consistently through use of Poisson's equation, and the values of the parameters $n_0 = e^{-\gamma-1}$, β, and ω must be chosen so that integrals of the density yield the specified values of N, E, and M. Most of this paper is concerned with characterizing such self-consistent solutions. Although thermal equilibria described by Eq. (2) have been studied before,[3-5] the significance of the parameter ω and interesting nonaxisymmetric solutions in a bounded domain have been overlooked.

A similar characterization has previously been provided for the thermal equilibrium configuration of a magnetically confined, non-neutral plasma column when all $3N$ degrees of freedom are retained. In this case, the distribution function is given by[6]

$$f(\mathbf{r},\mathbf{v}) = n_0\left(\frac{m\beta}{2\pi}\right)^{3/2} \exp\left\{-\beta\left[\frac{m}{2}(\mathbf{v}+\omega r\hat{\theta})^2 + q\phi + \frac{m\omega}{2}\left(\frac{qB}{mc}-\omega\right)r^2\right]\right\}. \tag{3}$$

For self-consistent solutions, the parameters n_0, β, and ω have been related to the total charge, energy, and angular momentum (including the kinetic terms).[7] As one would expect, the high-field limit ($qB/mc \gg \omega$) of the density $n = \int d^3\mathbf{v} f$ is identical in form to the guiding-center density, Eq. (2).

The distributions in Eqs. (2) and (3) are both of the form $C\exp(-\beta h_R)$, where $h_R = h + \omega p_\theta$ is the one-particle Hamiltonian in a frame rotating with frequency $-\omega$. For Eq. (3), h and p_θ refer to full three-degree-of-freedom dynamics; for Eq. (2), to the guiding-center dynamics alone. ω specifies a frame in which the density is static and does not respond secularly to static perturbations. Of course, the density of a symmetric plasma is static in any rotating frame, but there is a preferred frame for the asymmetric equilibria discussed below. As we shall see, ω need not actually equal the local $\mathbf{E}\times\mathbf{B}$ rotation rate anywhere in the guiding center fluid. The form of Eq. (1) and comparison with Eq. (3) shows that β can be identified as the inverse temperature.

The inverse temperature β is negative at large energies of the guiding-center system. (As noted by Onsager,[8] higher energy requires that the rods be packed together tightly; such states are characterized by greater order and hence lower entropy than more diffuse configurations, so $\beta = \partial S/\partial E < 0$.) There is an extensive literature on negative-temperature states of 2-D guiding-center systems and of formally identical systems of line vortices.[9-14,3] Our mean-field analysis follows most closely the previous work of Joyce and Montgomery[9] and Pointin and Lundgren.[13] This approach is particularly useful for a single-species plasma, since the mean-field density distribution is nontrivial (i.e., not a constant) even for positive β. In contrast to a neutral plasma, a single-species plasma can reach thermal equilibrium while confined magnetically.[15]

We will find that for energies above an angular-momentum-dependent threshold, corresponding to a certain range of negative β, the thermal equilibria do not share the underlying symmetry of the confinement geometry. The reason for this is easy to understand. Large energy requires the proximity of many rods, which can be realized by symmetric equilibria dominated by a small central cluster. However, the fixed mean-square radius associated with a given value of M implies the presence of a halo of particles at larger radii. (There is a finite limit to the energy of a thin annulus at the root-mean-square radius.) Symmetric configurations with two populations have less mean-field entropy than a single cluster displaced from the origin, so we expect off-axis configurations to predominate at large E. (Moreover, symmetric states with these energies are usually subject to diocotron instabilities; such instabilities furnish a mechanism for increasing entropy.) These off-axis equilibria are stationary not in the laboratory frame, but in a frame rotating with a frequency close to $-2Nqc/BLR^2$, which is the frequency of the $l = 1$ diocotron mode.[16]

Previous work on guiding-center thermal equilibria has concentrated on neutral systems, where the positive β mean-field equilibria are spatially homogeneous and have a well-defined thermodynamic limit. At high energy (and negative β), the rods tend to segregate into clusters of like charges. One may regard the transition between these kinds of equilibria as the spontaneous excitation of a low-order, zero-frequency mode. In a periodic system, the mode breaks the translational symmetry, much as the diocotron mode breaks the rotational symmetry in the present context.[13]

The off-axis states can also be understood in terms of a simple physical picture. From the form of the Boltzmann distribution [Eq. (2)], one can see that changing the sign of beta from positive to negative effectively changes the interaction between like charges from repulsive to attractive. Thus the effective potential may be decomposed into the local self-attraction of the cloud and a repulsive field or potential hill due to the image charges associated with the boundary condition. The ωr^2 term (for $\omega > 0$) represents a centered potential hill. The cloud can be confined between the two hills at a radius D, where $0 < D < R$; self-attraction then localizes it in azimuth.

This picture suggests that the symmetry is broken continuously—the equilibrium state is a continuous function of energy. In this sense, the transition between symmetric and off-axis states of maximum entropy resembles a second-order phase transition. (Some aspects of this analogy have been presented elsewhere.[1]) Indeed, as we show below, certain thermodynamic derivatives change discontinuously, and significant fluctuations of the displacement mode persist near the transition in the limit of large N. Fluctuations are also important near transitions in neutral guiding-center systems, which have been studied from a different point of view by Lundgren and Pointin.[14]

The remainder of this paper is organized as follows. Some of the properties of mean-field thermal equilibria are explored in Sec. II. Section III is devoted to the thermodynamic stability of such equilibria. In Sec. IV, we compare the predictions of mean-field theory with Monte Carlo simulations of the discrete system, and discuss the importance of fluctuations near the transition. Some of the unusual thermodynamic properties of the system are discussed in Sec. V. We conclude with a discussion of the implications of this study. Details of the bifurcation theory of solutions to the mean-field equations are presented in the Appendix A, as are the numerical methods used for various parts of this project.

II. MEAN-FIELD THEORY

Before proceeding with the mean-field analysis, it is useful to introduce scaled variables. We scale lengths by R, densities by (N/R^2L), potentials by (qN/L), energies by (N^2q^2/L), and angular momenta by $(qNBR^2/2c)$. In terms of the scaled variables, Poisson's equation takes the form $\nabla^2\phi = -4\pi n$, with the boundary condition $\phi = 0$ at $r = 1$, and the conserved quantities are given by

$$1 = \int d^2\mathbf{r}\, n, \quad E = \frac{1}{2}\int d^2\mathbf{r}\, n\phi, \quad M = \int d^2\mathbf{r}\, r^2 n. \tag{4}$$

Note that M is now explicitly the mean-squared radius. Similarly, the entropy per rod is $S = \int d^2\mathbf{r}\, n \ln n - \ln(N/R^2L)$; since the last term is a constant, it may be dropped. Note that all explicit dependence on N, R, and B has been removed through this scaling. The entropy per rod is extremized subject to Eqs. (4) by densities satisfying

$$n(\mathbf{r}) = n_0 \exp\{-\beta[\phi(\mathbf{r}) + \omega r^2]\}$$
$$= n_0 \exp(4\pi\beta\nabla^{-2}n - \omega\beta r^2). \tag{5}$$

Here, β is the inverse temperature scaled by (L/Nq^2); this scaling is a reminder that the large N limit is not described by a conventional thermodynamic limit. The rotation frequency ω is scaled by $(2cNq/LR^2B)$, which is the $\mathbf{E}\times\mathbf{B}$ drift rotation frequency at the boundary (for the case of a cylindrically symmetric column), and also the frequency of the $l = 1$ diocotron mode. These scalings are associated with invariances of Eq. (5) under $(n_0 \to an_0, \beta \to \beta/a)$ and $(r \to br, \omega \to \omega/b^2, n_0 \to n_0/b^2)$. Again, n_0, ω, and β are to be determined from the constraints, Eqs. (4). Thermal equilibria thus form a two-parameter family, specified as $n = n(\mathbf{r};E,M)$, $\beta = \beta(E,M)$, and $\omega = \omega(E,M)$.

Equation (5) may be derived as an approximate description of the microcanonical ensemble of the discrete system by several methods, e.g., by counting areas in phase space,[9,3] or expanding the hierarchy of static correlation functions in powers of the plasma parameter.[11,14] It is worth emphasizing that all such derivations assume certain correlations are weak; we will return to this point. Finite boundaries and/or an angular momentum constraint allow for thermal equilibria with a nontrivial mean field. This is what allows for interesting results at the level of a distribution function of the Boltzmann type.

Let us choose a representative value of angular momentum, say $M = 0.1$, and follow the behavior of the equilibrium as a function of energy. β, ω, and S are plotted as functions of E in Figs. 1–3. The points marked A–D have been selected as illustrative limits; some of the state variables corresponding to these points are listed in Table I, and they are discussed more fully below. All solutions up to point D are symmetric, so they satisfy the equation

$$\frac{1}{r}\frac{d}{dr}r\frac{d}{dr}\ln n(r) = 4\pi\beta n - 4\beta\omega, \tag{6}$$

subject to a regularity condition $n'(0) = 0$, with $n(0)$, β, and ω chosen to satisfy Eqs. (4). For computational pur-

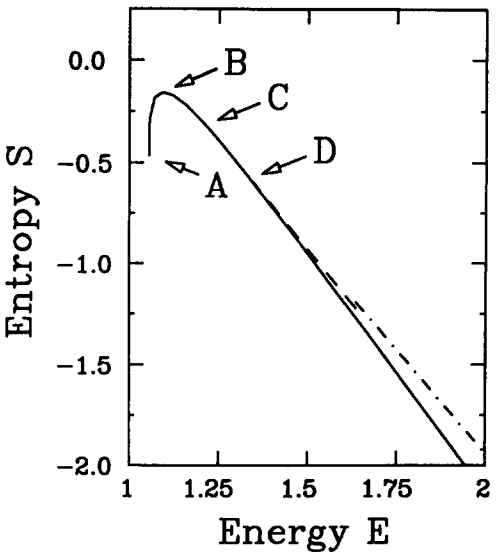

FIG. 1. Dependence of entropy on energy, for mean-field equilibria [solutions of Eq. (5)], at fixed $M = 0.1$. The solid line represents the symmetric branch; the dashed line, results of (perturbative) bifurcation theory; the dot-dashed line, the large-energy approximation described in the text. The points marked A–D are discussed in the text.

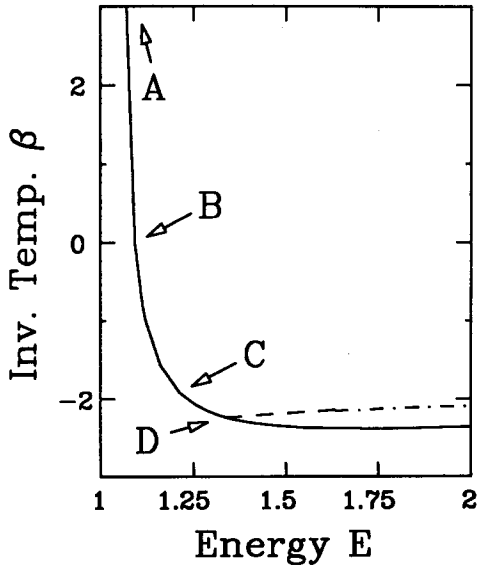

FIG. 2. Dependence of inverse temperature on energy; parameters and conventions as in Fig. 1.

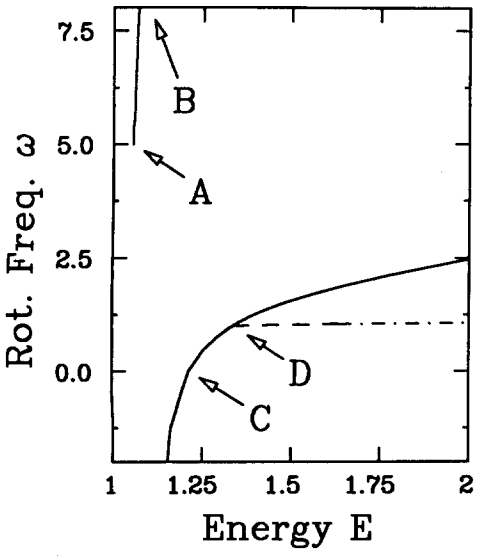

FIG. 3. Dependence of rotation frequency on energy; parameters and conventions as in Fig. 1.

poses, it is most convenient to solve Eq. (6) indirectly, by integrating

$$\frac{1}{r}\frac{d}{dr}r\frac{d}{dr}u = fe^u - g, \quad u(0)=0, \quad u'(0)=0, \tag{7}$$

numerically, for specified constants f and g. Then an equilibrium is given by $n(r) = C \exp u(r), \beta = Cf/4\pi$, and $\omega = g/4\beta$, where $C^{-1} = 2\pi\int_0^1 dr\, ru(r)$. A standard root-finding algorithm was used to adjust f or g to achieve the desired value of M, and other quantities calculated from the solution were used for the plots. An alternative method, described in Appendix C, gives equivalent results and can also be used to find asymmetric equilibria, but is not as accurate because it employs a fixed spatial grid.

Point A corresponds to zero temperature ($\beta \to +\infty$), where the density profile is a step function, $n(r) = \frac{1}{2}\pi M$ for $r < \sqrt{2M}$, $n(r) = 0$ for $r > \sqrt{2M}$. This profile minimizes the energy for the specified values of total charge and angular momentum, so point A is the lower limit of the curves in Figs. 1–3.

For slightly larger energies, the outside edge of the profile is rounded over a scale length set by the Debye length $\lambda_D = [4\pi\beta n(0)]^{-1/2}$, which is approximately $(M/2\beta)^{1/2}$ in our units. Such profiles are identical to those discussed previously[7] as positive-temperature states of a $3N$-degree-of-freedom plasma.

Point B represents the limit of the profile rounding, where $\beta \to 0$ but $\omega \to \infty$ simultaneously so that the limit of $\omega\beta$ is finite. The density profile becomes Gaussian, $n(r) = n_0 e^{-\beta\omega r^2}$. Since $\beta = \partial S/\partial E$, point B is the maximum of the curve $S(E)$ and corresponds to infinite temperature, which cannot be attained in a $3N$-degree-of-freedom plasma.

At point C, where the rotation frequency vanishes, Eq. (6) may be solved exactly. [For instance, by transforming to new variables $\eta = \ln r$ and $y(\eta) = \ln n(r) + 2\eta$, one can integrate to obtain a Riccati equation for $y'(\eta)$.] The result for $\beta < 0$ is

$$n(r) = 4A/(2 - \pi\beta A r^2)^2. \tag{8}$$

The constraints yield the relations

$$A = n(0) = [\pi(1 + \tfrac{1}{2}\beta)]^{-1}, \tag{9a}$$

$$M = \left(1 + \frac{2}{\beta}\right)\left[1 - \frac{2}{\beta}\ln\left(1 + \frac{\beta}{2}\right)\right], \tag{9b}$$

and

$$E = -\frac{2}{\beta^2}\left[\ln\left(1 + \frac{\beta}{2}\right) - \frac{\beta}{2}\right]. \tag{9c}$$

Equation (8) was introduced as an approximation in Ref. 4, in the context of a point-vortex system without boundaries. Note that as $M \to 0$, i.e., the system shrinks to a point, the inverse temperature approaches the value -2. This corresponds to the "supercondensation" phenomenon described by Kraichnan.[17] We will return to the thermodynamic significance of equilibria described by Eq. (8) in Sec. V.

TABLE I. State functions (energy E, inverse temperature β, rotation frequency ω, and entropy S) for representative mean-field thermal equilibria, at angular momentum $M = 0.1$.

Label	E	β	ω	S
A	$\frac{1}{4} - \frac{1}{2}\ln(2M) \approx 1.055$	∞	$(2M)^{-1} = 5.0$	-0.200
B	1.093	0	$\pm\infty$	-0.158
C	1.213	-1.917	0	-0.318
D	1.337	-2.232	1	-0.579
E	∞	-2	$(1-M)^{-1} \approx 1.111$	$-\infty$

A. A continuation algorithm

Before discussing the transition point D, it is convenient to describe a formal procedure for progressing along the curves in Figs. 1–3. That is, we start at one solution n of Eq. (5) at specified (M,E) and advance to a nearby solution $n + \delta n$ at the energy $E + \delta E$. The density has the form $n = \exp(-\beta\phi - \alpha r^2 - \gamma)$, where $\alpha = \beta\omega$ and $\gamma = -\ln n_0$. We compute the density increment perturbatively. Ordinarily, the leading terms in δn are $\mathcal{O}(\delta E)$:

$$\delta n = -n(\delta\beta\,\phi + r^2\,\delta\alpha + \delta\gamma + \beta\,\delta\phi) + \mathcal{O}(\delta E^2), \tag{10}$$

where $\delta\phi$ satisfies $\nabla^2\,\delta\phi = -4\pi\,\delta n$, $\delta\phi = 0$ at $r = 1$, and the increments $(\delta\alpha,\delta\beta,\delta\gamma)$ are to be computed from the constraints at consistent order:

$$0 = \int d^2\mathbf{r}\,\delta n, \tag{11a}$$

$$\delta E = \int d^2\mathbf{r}\;\phi\,\delta n + \mathcal{O}(\delta E^2), \tag{11b}$$

and

$$0 = \int d^2\mathbf{r}\,r^2\,\delta n. \tag{11c}$$

Ordinarily, we can eliminate the parameter increments by substituting Eq. (10) into Eq. (11):

$$\begin{pmatrix} 0 \\ \delta E \\ 0 \end{pmatrix} + \beta \int d^2\mathbf{r}\, n\, \delta\phi \begin{pmatrix} r^2 \\ \phi \\ 1 \end{pmatrix} = -\mathbf{M} \begin{pmatrix} \delta\alpha \\ \delta\beta \\ \delta\gamma \end{pmatrix}, \tag{12}$$

where the matrix $\mathbf{M}$ is given by

$$\mathbf{M} = \int d^2\mathbf{r}\, n \begin{pmatrix} r^4 & r^2\phi & r^2 \\ r^2\phi & \phi^2 & \phi \\ r^2 & \phi & 1 \end{pmatrix}, \tag{13}$$

and terms of $\mathcal{O}(\delta E^2)$ are neglected in this paragraph. Hence

$$\begin{pmatrix} \delta\alpha \\ \delta\beta \\ \delta\gamma \end{pmatrix} = -\mathbf{M}^{-1} \begin{pmatrix} 0 \\ \delta E \\ 0 \end{pmatrix} - \beta \mathbf{M}^{-1} \int d^2\mathbf{r}\, n\, \delta\phi \begin{pmatrix} r^2 \\ \phi \\ 1 \end{pmatrix}. \tag{14}$$

Equation (10) and Poisson's equation then yield

$$\mathscr{L}\,\delta\phi = 4\pi n(\mathbf{r}) A(\mathbf{r}) \delta E, \tag{15}$$

where

$$\mathscr{L} = \nabla^2 - 4\pi n\beta(1 + r^2\mathscr{L}_\alpha + \phi\mathscr{L}_\beta + \mathscr{L}_\gamma), \tag{16}$$

$$\begin{pmatrix} \mathscr{L}_\alpha(\delta\phi) \\ \mathscr{L}_\beta(\delta\phi) \\ \mathscr{L}_\gamma(\delta\phi) \end{pmatrix} = -\mathbf{M}^{-1} \int d^2\mathbf{r}\, n\, \delta\phi \begin{pmatrix} r^2 \\ \phi \\ 1 \end{pmatrix}, \tag{17}$$

and

$$A(\mathbf{r}) = -[r^2(\mathbf{M}^{-1})_{12} + \phi(\mathbf{M}^{-1})_{22} + (\mathbf{M}^{-1})_{32}]. \tag{18}$$

This algorithm will fail if there is a singularity in the linear problems posed above. A singularity of the operator $\mathscr{L}$ (vanishing eigenvalue) can lead to bifurcation, that is, a confluence of multiple solution branches. Just this situation occurs at the transition point. If the matrix $\mathbf{M}$ is singular, then there is ambiguity in the parameters α,β,γ. The only case of this kind of singularity which we have encountered is associated with a degenerate bifurcation from a spatially uniform density. Although we have analyzed this case, we do not discuss it here, because it does not lead to maximum-entropy equilibria (cf. Sec. III).

B. The transition point

At a bifurcation, we must retain higher-order terms in the perturbation analysis to obtain consistent solutions when $\delta\phi$ involves a singular eigenfunction ψ of $\mathscr{L}$. First we characterize ψ itself.

Since the basic solution n is on the axisymmetric branch, the linear problem $\mathscr{L}\psi = 0$ can be decomposed into azimuthal Fourier harmonics, labeled by mode number l. Here we assume the bifurcation involves a change of symmetry ($l > 0$); the special case of $l = 0$ is discussed in Appendix B. Let the first-order potential increment be $x\psi(r,\theta)$, where ψ is normalized independently of $x, \partial^2\psi/\partial\theta^2 = -l^2\psi$, and x is an amplitude. Then we note that the azimuthal phase, and *a fortiori* the sign, of ψ are arbitrary. Thus the parameters $\delta\alpha$, $\delta\beta$, $\delta\gamma$ must be invariant under the operation $x \to -x$. At leading order, the constraints are satisfied trivially because of the azimuthal dependence, so δE, δM, $\delta\alpha$, $\delta\beta$, and $\delta\gamma$ are $\mathcal{O}(x^2)$, and ψ satisfies $\mathscr{L}_l\psi = 0$, $\psi = 0$ at $r = 1$ and regular at the origin. The effective linear operator $\mathscr{L}_l$ is defined by

$$\mathscr{L}_l f = \left(\frac{1}{r}\frac{d}{dr} r \frac{d}{dr} - \frac{l^2}{r^2}\right) f - 4\pi\beta n f. \tag{19}$$

Here we restrict our attention to the $l = 1$ Fourier subspace; other values of l are irrelevant for reasons of thermodynamic stability, as we show below. Hence we let $\psi = \hat{\psi}(r)e^{i\theta} + \text{c.c.}$, and look for a solution of the equation

$$\left(\frac{1}{r}\frac{d}{dr} r \frac{d}{dr} - \frac{1}{r^2}\right)\hat{\psi} - 4\pi\beta n\hat{\psi} = 0. \tag{20}$$

It is illuminating to rewrite Eq. (20) in the form

$$\left(\frac{1}{r}\frac{d}{dr} r \frac{d}{dr} - \frac{1}{r^2}\right)\hat{\psi} + \frac{2\pi}{r}\frac{dn}{dr}\left(\frac{1}{2r}\frac{d\phi}{dr} + \omega\right)^{-1}\hat{\psi} = 0, \tag{21}$$

which is just the dispersion relation for an $l = 1$ diocotron mode in terms of the scaled variables. The $\mathbf{E}\times\mathbf{B}$ velocity is $\frac{1}{2}\hat{z}\times\nabla\phi$ in these units, so the local $\mathbf{E}\times\mathbf{B}$ rotation rate of the equilibrium is $\omega_E(r) = (\frac{1}{2}r)(d\phi/dr)$. This quantity is negative, and at the wall has the value $\omega_E(1) = -1$. For $\omega = 1$, the frequency of the $l = 1$ diocotron mode, Eq. (21) has a smooth solution satisfying the boundary condition $\hat{\psi}(1) = 0$, given by[16]

$$\hat{\psi} = Dr[\omega_E(r) + 1], \tag{22}$$

where D is a constant. Substituting this expression into the second term of Eq. (21), and using the Laplacian in the first term to compute the associated density perturbation, yields

$$\delta n(r,\theta) = \frac{dn}{dr}|D|\cos(\theta + \arg\mathbf{D}). \tag{23}$$

Thus, to first order in D, a step along the asymmetric branch is simply a displacement of the column away from the axis.

To see why the bifurcation occurs at $\omega = 1$, recall the interpretation of the off-axis column as a self-attracting cluster of rods trapped between the ωr^2 potential hill and the image charge associated with the conducting wall. A small displacement $\mathbf{D}$ gives rise to a dipole image potential $\phi_I = -2\mathbf{D}\cdot\mathbf{r}$. The average force on a rod due to the potential hill is $N^{-1}\Sigma_j\nabla_j\omega r_j^2 = 2\omega\mathbf{D}$, and the average force due to the image potential is $N^{-1}\Sigma_j\nabla_j(-2\mathbf{D}\cdot\mathbf{r}_j) = -2\mathbf{D}$, where we have used the normalization $N^{-1}\Sigma_j 1 = \int d^2\mathbf{r}\, n(r) = 1$ for both terms. Thus force balance yields the condition $\omega = 1$.

In Appendix A, we relate the branches near the bifurcation to solutions of a nonlinear algebra problem of the form $Ax + x^3 = 0$, which describes a pitchfork bifurcation for the amplitude x in terms of a bifurcation parameter A, which is generically proportional to a linear combination of δM and δE. The analysis also furnishes perturbative expressions for the dependence of β and ω on E along the off-axis branch, which were used to construct the dashed curves in Figs. 1–3.

C. Large energies

When the energy is sufficiently large (for a fixed value of M), the most probable density distribution is localized within a region of small radius r_p, much smaller than the magnitude of the displacement $\mathbf{D}$ of the center of charge. If the cloud is sufficiently far from the wall [$r_p \ll (1 - D)$], an

approximate description of an asymmetric equilibrium density $n(r,\theta;\beta,n_0,\omega)$ may be constructed as follows. Letting $\mathbf{r}' = \mathbf{r} - \mathbf{D}$, we write the potential as $\phi(\mathbf{r}) = \phi_I(\mathbf{r}') + \phi_P(\mathbf{r}')$, where $\phi_I(\mathbf{r}') = 2\ln|\mathbf{r}D - \mathbf{D}/D|$ is the image potential of a unit charge at $\mathbf{D}$. This is very nearly the image potential of the cloud itself, which is assumed to be localized away from the wall. The boundary condition $\phi(r=1,\theta)=0$ requires that $\phi_P \sim -2\ln|\mathbf{r}-\mathbf{D}|$ for $|\mathbf{r}-\mathbf{D}| \gg r_p$.

We rewrite Poisson's equation as

$$\nabla'^2\phi_P = -4\pi n_0 \times \exp[-\beta(\phi_P + \omega r'^2 + 2\omega \mathbf{r}'\cdot\mathbf{D} + \omega D^2 + \phi_I)]. \tag{24}$$

To find a solution in the vicinity of the plasma, we Taylor expand in r':

$$\phi_I(\mathbf{r}') \sim 2\ln|1-D^2| - \frac{2\mathbf{D}\cdot\mathbf{r}'}{1-D^2}. \tag{25}$$

It is convenient to let

$$n_0' = n_0 \exp[-\beta(2\ln|1-D^2| + \omega D^2)], \tag{26}$$

and to choose $\omega = 1/(1-D^2)$, so that Eq. (24) reduces to

$$\nabla'^2\phi_P = -4\pi n_0' \exp\{-\beta[\phi_P(\mathbf{r}') + \omega r'^2]\}. \tag{27}$$

Note that this choice for ω is equivalent to the force balance condition $2\omega\mathbf{D} + \nabla'\phi_I = 0$ at $r' = 0$. The large r' asymptotic behavior $\phi_P(r',\theta') \sim -2\ln r'$ is equivalent to the boundary condition $\phi_P(r'=1,\theta')=0$, and the constants n_0' and β are determined by the constraints

$$1 = \int d^2\mathbf{r}'\, n_0' \exp\{-\beta[\phi_P(\mathbf{r}') + \omega r'^2]\}, \tag{28a}$$

$$M' = \int d^2\mathbf{r}'\, r'^2 n_0' \exp\{-\beta[\phi_P(\mathbf{r}') + \omega r'^2]\}, \tag{28b}$$

where $M' = M - D^2$ is the portion of the canonical angular momentum due to the dispersion of charge around $\mathbf{D}$.

Consequently, we have reduced the large-displacement equilibrium problem to a radial integration: The desired solution of Eq. (27) is the symmetric one characterized by $\omega = 1/(1-D^2)$ and $M' = M - D^2$. This solution yields a cloud self-energy E', which we relate to the energy of the off-axis equilibrium through

$$E = \frac{1}{2}\int d^2\mathbf{r}\, n\phi = \frac{1}{2}\int d^2\mathbf{r}\, n\phi_I + \frac{1}{2}\int d^2\mathbf{r}\, n\phi_P = \ln(1-D^2) + E', \tag{29}$$

where $\ln(1-D^2)$ is the energy of interaction with the image charge. As D^2 approaches M, the plasma is concentrated into a small column with a large self-energy E'. Hence E can be substantially larger than the bifurcation value E_c. Note that the plasma becomes better localized as $D^2 \to M$, and the above approximations become more reliable. A thermodynamic interpretation of this scheme will be given in Sec. V. The results of the above approximation scheme are indicated by dot-dashed curves in Figs. 1–3. At very large energies, the column is so thin that $\exp(-\beta\omega r'^2)$ does not differ significantly from unity over the region of appreciable density. Thus a good approximation to the density distribution is given by the $\omega = 0$ solution, Eq. (8), for the appropriate value of M'. This leads to the asymptotic value of -2 for the inverse temperature β as $E \to \infty$ at any fixed M.

The symmetric solutions to the Euler–Lagrange equation for $E > E_c$ are not physically relevant, since they are not entropy maxima. (We argue below that they are not even relative maxima.) These solutions oscillate at large r; as the first radial minimum crosses $r = 1$ from the outside, we obtain the two-population configuration described earlier (central cluster and halo near the wall). But this is just where the bifurcation occurs, so such solutions compete with the off-axis ones. As energy increases, the separation between the two populations becomes more severe; a limit is continuously approached in which a fraction of the charge (equal to M) is arbitrarily close to the wall and the remaining charge is concentrated at the center. The limiting value of β along this branch as $E \to \infty$ is $-2/N(1-M)$, corresponding to the condensation temperature for the central cluster alone.

III. THERMODYNAMIC STABILITY

All of the solutions discussed above (symmetric and off-axis) are constrained extremals of the entropy. However, by the postulates of statistical thermodynamics, only entropy maxima are related to long-time averages. This requirement plays the role of thermodynamic stability for the microcanonical ensemble. As we show below, the principal $l = 1$ bifurcation discussed above is the first to occur as E is increased from its minimum value. There is only one extremal for $E < E_c$; this must be a constrained entropy maximum, since the entropy is bounded from above. Above E_c, we must determine which of the extremals is the maximum. A simple way to compare the two branches is to use the thermodynamic relation $dS = \beta(dE + \omega\, dM)$, which is easily verified for infinitesimal changes which preserve the total charge and satisfy the condition for an extremal ($\ln n = -\beta\phi - \beta\omega r^2 - \gamma$). For steps along either solution branch $dM = 0$, so $S(E) = S(E_c) + \int_{E_c}^{E}\beta(E)dE$, where $\beta(E)$ is evaluated along the branch in question. Since $\beta(E)$ is larger along the off-axis branch, that branch has larger entropy. At the bifurcation, thermodynamic stability is transferred from the symmetric branch to the off-axis one.

There are other branches of solutions to the extremal problem at larger energies. Nevertheless, we believe that the above description correctly describes the thermodynamically stable equilibria at all values of E, on the basis of a qualitative argument and numerical evidence. Since S is maximized by solutions with the least structure, we expect entropy maxima to have a single density peak (or well, for $M > 1/2$), as do the symmetric solutions for $E < E_c$ and the off-axis solutions for $E > E_c$. Furthermore, such solutions extend to arbitrarily large energies.

The signature of a local entropy maximum is the negative definiteness of the second-order change in the entropy, δS, for density perturbations which satisfy the constraints. Next we construct an explicit representation for δS, and show that the symmetric branch changes from a local maximum to a saddle of the entropy as E is increased through the

critical value. We also argue that the off-axis branch is a local maximum.

Let us consider the change in S associated with a small deviation δn from the equilibrium density n, to second order:

$$\delta S \sim -\int d^2\mathbf{r}(\ln n + 1)\delta n - \int d^2\mathbf{r}\,\frac{\delta n^2}{2n}. \tag{30}$$

We require that δn not change the charge, angular momentum, or energy:

$$0 = \int d^2\mathbf{r}\,\delta n, \tag{31a}$$

$$0 = \int d^2\mathbf{r}\,r^2\,\delta n, \tag{31b}$$

$$0 = \int d^2\mathbf{r}(\phi\,\delta n + \tfrac{1}{2}\delta n\,\delta\phi). \tag{31c}$$

and

By substituting $\ln n = -\alpha r^2 - \beta\phi - \gamma$, using the constraints and Poisson's equation, we find that

$$\delta S \sim -\frac{1}{32\pi^2}\int d^2\mathbf{r}\left(\frac{\nabla^2\delta\phi}{n} - 4\pi\beta\,\delta\phi\right)\nabla^2\delta\phi. \tag{32}$$

[Of course, the first-order change around a constrained extremal vanishes for any δn satisfying the first-order constraints, Eqs. (31a) and (31b) and $\int d^2\mathbf{r}\,\phi\,\delta n = 0$.] The quantity in large parentheses is closely related to the eigenvalue problem

$$\nabla^2\psi_\nu - 4\pi n(\beta + \lambda_\nu)(1 + r^2\mathcal{L}_\alpha + \phi\mathcal{L}_\beta + \mathcal{L}_\gamma)\psi_\nu = 0, \tag{33}$$

with $\psi_\nu = 0$ at the boundary $r = 1$. Recall that the functionals $\mathcal{L}_\alpha$, $\mathcal{L}_\beta$, and $\mathcal{L}_\gamma$ [see Eq. (17)] are constructed so that the density perturbation $n_\nu = -(4\pi)^{-1}\nabla^2\psi_\nu$ satisfies the first-order constraints. An appropriate inner product for potential perturbations is $(f,g) = \int d^2\mathbf{r}\,\nabla f\cdot\nabla g$. From Eq. (33) and the constraints, it is easily seen that $(\lambda_\nu - \lambda_\mu)(\psi_\nu,\psi_\mu) = 0$, so the ψ_ν can be chosen to satisfy the orthonormality condition $(\psi_\nu,\psi_\mu) = 4\pi\delta_{\nu\mu}$. We will assume that they are complete in the space of normalizable functions which satisfy the constraints and vanish on the boundary. (If they are not, a variational interpretation of the eigenvalue problem justifies our criterion for definiteness.) Accordingly, we expand any allowed potential perturbation as $\delta\phi = \Sigma_\nu a_\nu\psi_\nu$; by substituting into Eq. (32), and using the constraints and orthonormality, we find that $\delta S = \frac{1}{2}\Sigma_\nu\lambda_\nu a_\nu^2$ to second order. That is, the λ_ν are generalized eigenvalues of the second variational operator $\delta^2 S/\delta n^2$. If the algebraically largest eigenvalue is negative, n furnishes a local maximum of the entropy.

For $\lambda = 0$, Eq. (33) reduces to $\mathcal{L}\psi = 0$, which was introduced earlier as the criterion for bifurcation. Hence the second variation has a zero eigenvalue at the critical energy $E = E_c$. There are two singular eigenfunctions, which are proportional to linear combinations of $\sin\theta$ and $\cos\theta$. Since there are no zero eigenvalues for $E < E_c$, and the symmetric branch is stable for sufficiently small E, all eigenvalues are negative for $E < E_c$. As E increases through E_c, the doubly degenerate principal $l = 1$ eigenvalue increases through zero, and the symmetric branch changes from an entropy maximum to a saddle. We have evaluated various eigenvalues along the symmetric branch numerically (using a scheme described in Appendix B). The results shown in Fig. 4 confirm $l = 1$ stability below E_c and instability above, for the representative case of $M = 0.1$. (For $l > 1$, stability also follows from Sturm–Liouville theory.) The principal eigenvalue for $l = 0$ is always negative at the bifurcation, as shown in Fig. 5.

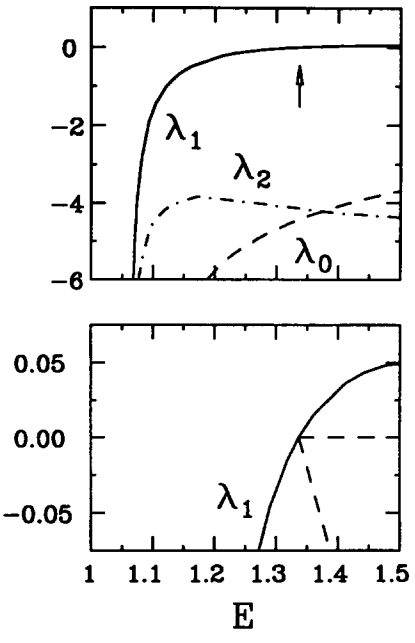

FIG. 4. Eigenvalues of the second variation $\delta^2 S/\delta n^2$ as a function of scaled energy, for equilibria with $M = 0.1$. Top: axisymmetric equilibria, principal eigenvalues λ_l for $l = 0,1,2$. Bottom: principal eigenvalues near the bifurcation (solid line, symmetric branch; dashed lines, off-axis branch).

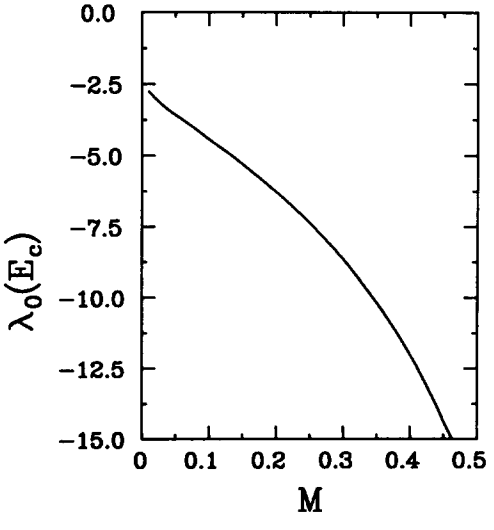

FIG. 5. Principal $l = 0$ eigenvalue of $\delta^2 S/\delta n^2$ at the critical energy, for various angular momenta M.

On the off-axis solution branch, the degeneracy is broken. One eigenvalue remains zero; the associated eigenfunction is $\partial\phi/\partial\theta$, corresponding to an infinitesimal change of the azimuthal phase of the equilibrium, which obviously does not affect any scalar state variables. The perturbative numerical evaluation of the other eigenvalue (see Appendix A) shows that it is negative, as shown in Fig. 4(b). Hence this branch represents rotationally degenerate, local maxima of the constrained entropy.

This situation is analogous to the well-known connection between bifurcation and stability of dynamical systems, with the appropriate interpretation of the eigenvalues. Once the rotational degeneracy has been factored out, this is a forward pitchfork bifurcation, with E as the bifurcation parameter. Accordingly, one expects a transfer of stability from the symmetric to the off-axis branch.

The similarity between our variational problem and that which arises in Arnol'd's method for treating nonlinear dynamical stability[18,19] suggests a nontrivial property of the displaced equilibria in the continuum limit. By the complementarity property of constrained extrema, the mean-field thermal equilibria are energy maxima at fixed entropy; since energy and entropy are conserved by the incompressible $\mathbf{E}\times\mathbf{B}$ flow, all small perturbations should be benign. Specifically, they lead to evolution which can be decomposed into a change of azimuthal phase and a residual which must remain small.

IV. MONTE CARLO SIMULATIONS

To check the predictions of the mean-field theory, we have simulated representative microcanonical ensembles numerically. We used a modification of Creutz's microcanonical Monte Carlo algorithm.[20] The simulation consists of an ensemble of configurations consisting of N points $\{\mathbf{r}_j\}$ in the unit disk, plus an auxiliary degree of freedom, known as a demon, which is characterized entirely by its energy E_D and its angular momentum M_D. The demon parameters are constrained to be in narrow ranges $|E_D| < E_M, |M_D| < M_M$. The total energy includes particle–particle and particle–image interactions, and is given by

$$E_T = E_D - \sum_{i\neq j} \ln\left(|\mathbf{r}_i - \mathbf{r}_j|\right) + \sum_{i,j} \ln\left(r_j|\mathbf{r}_i - r_j^{-2}\mathbf{r}_j|\right) . \tag{34}$$

Here, E_T is conserved to within roundoff error for each ensemble. Similarly the total angular momentum $M_T = M_D + \Sigma_j r_j^2$ is conserved. We construct a sequence of configurations within errors E_M and M_M of the energy-momentum shell which defines a microcanonical ensemble with specified values E_T and M_T. An initial configuration is established by annealing. A candidate for a step to another configuration is constructed by using a random number generator to pick two distinct particle indices i and j, and displacements $\delta\mathbf{r}_i$, $\delta\mathbf{r}_j$ uniformly distributed on a square of edge Δ. (Displacements which would leave the disk are rejected.) The changes in energy and angular momentum associated with the displacements are computed; the new configuration is accepted if and only if these amounts can be transferred to the demon without exceeding its parameter ranges. Evolution via this sort of "long-range collision" between two particles is more efficient than single-particle moves, since it allows for more rapid radial motion without violating the fixed value of mean-square radius. A "Monte Carlo step per particle," (MCS) consists of N such collisions. The step scale Δ is adjusted to maintain a rejection ratio consistent with efficient exploration of phase space. Statistics are collected over ensembles of typically 40 000 MCS.

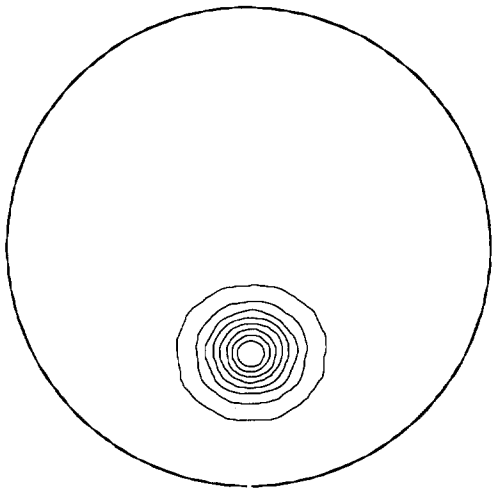

FIG. 6. Density contours in the high-energy phase, at $M = 0.3$ and $E = 0.9$, from a Monte Carlo simulation with 512 rods. The rod locations were accumulated over 10 000 configurations, in a coordinate system with the net dipole moment for each configuration directed downward.

Examination of typical realizations at large energies shows that they are indeed displaced from the center. The average density $n_{\mathrm{MC}}(r,\theta)$ (with the center of charge at $\theta = 0$) was computed for some of the Monte Carlo runs. An example of contours of n_{MC} in the displaced phase are shown in Fig. 6, along with the corresponding mean-field equilibrium in Fig. 7, which was approximated numerically using a

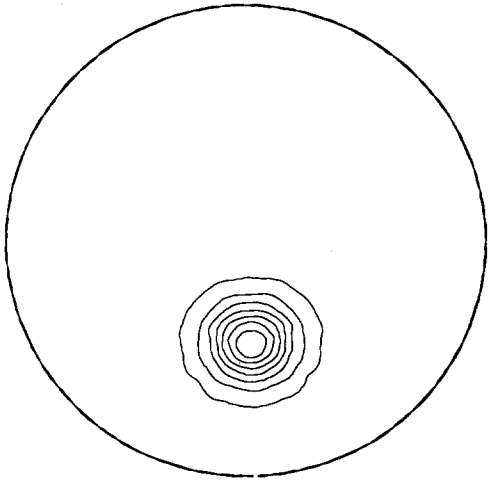

FIG. 7. Density contours at $M = 0.3$, $E = 0.9$, from numerical solution of the mean-field equation.

method described in Appendix C.

As noted by Creutz, the demon is effectively in thermal equilibrium with a heat bath when N is large. Its energy and angular momentum distributions therefore tend to the forms $\exp(-\beta E_D/N)$ and $\exp(-\beta\omega M_D/N)$. (Recall from Sec. II that beta differs by a factor of N from the usual inverse temperature; for the simulations, L and q were set equal to unity.) Hence the demon parameters must be bounded on one side, in accordance with the signs of β and ω. A second bound is used to ensure faithful approximation of the microcanonical ensemble for moderate N; that is, E_M and M_M must be chosen small enough that relative fluctuations in E and M are negligible. On the other hand, they should be large enough to allow for efficient progress through the allowed region of phase space. The parameters β and ω are determined by fitting the observed distributions of E_D and M_D to exponentials; the results are shown as functions of energy in Figs. 8 and 9. For our data, the accuracy of this technique is limited to about 1% and 5% for β and ω, respectively, as determined from a chi-squared test. We have checked that the results are not significantly affected by moderate changes in E_M and M_M.

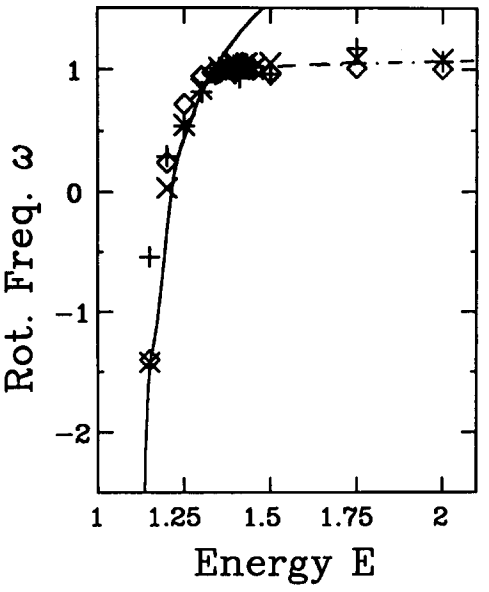

FIG. 9. Dependence of rotation frequency on energy for $M = 0.1$, as inferred from Monte Carlo simulations. Symbols as in Fig. 8.

A. The order parameter

To quantify the asymmetry, it is convenient to introduce as an order parameter the mean dipole moment per particle, $D = |\Sigma_j \mathbf{r}_j|/N$. Here D is proportional to the amplitude x of the spontaneously excited fundamental diocotron mode, which arose in the bifurcation analysis. The dependence of ensemble averages of D on energy are shown in Fig. 10. In the symmetric phase, $\langle D \rangle$ has a small value associated with thermal fluctuations of order $N^{-1/2}$. In the displaced phase, $\langle D \rangle$ is nearly independent of N and grows slowly to the maximum value consistent with M. The Monte Carlo results for $\langle D \rangle$ appear to be consistent with mean-field theory, although discrepancies in the immediate vicinity of the transition cannot be ruled out.

B. Fluctuations near the transition

The mean-field approach of the previous section may be regarded as a weak-correlation approximation. This approximation may break down in several ways. There may be long-lived dynamical correlations which make the ergodic hypothesis inapplicable on the time scales of interest; we will not consider this case here. At sufficiently low energies, correlations on the scale of the interparticle separation become

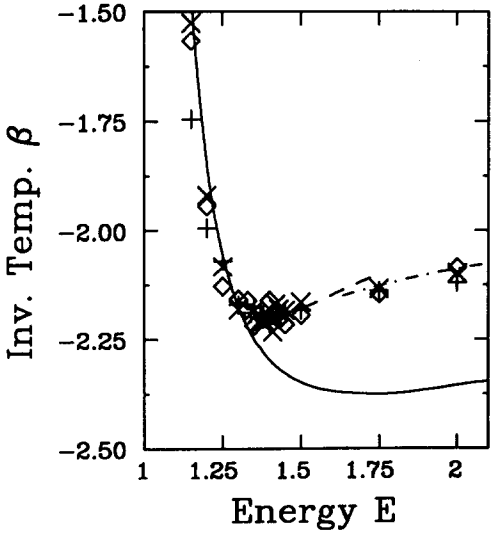

FIG. 8. Dependence of inverse temperature on energy for $M = 0.1$, as inferred from Monte Carlo simulations. Symbols: $+$, $N = 256$; $\times$, $N = 512$; $\diamond$, $N = 1024$. Other conventions as in Fig. 1.

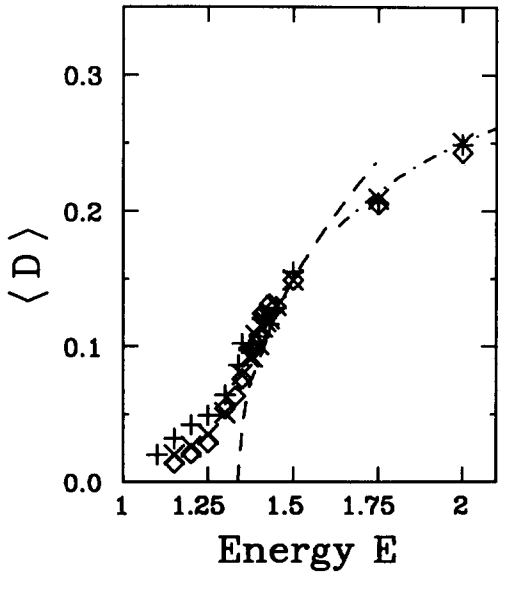

FIG. 10. The order parameter (dipole moment) from the Monte Carlo simulations and mean-field theory. Symbols as in Fig. 8.

important. These ultimately lead to the frustrated triangular lattices described by Stauffer and Fetter,[21] but are not of concern in the present context. Near the bifurcation, one of the second variation eigenvalues is very small. That is, the configurations with macroscopic amplitudes of the displacement mode are not much less probable than the maximum-entropy states, and averages may deviate substantially from the most probable values. This is analogous to critical behavior near a second-order phase transition.

The dominant fluctuations can be measured by the variance of the dipole moment. In the continuum approximation, the probability $\mathscr{P}(n)$ of a configuration n is proportional to $(\exp NS\{n\})$. Thus a schematic expression for the ensemble average of a state functional $A\{n\}$ is given by

$$\langle A\rangle = \int \mathscr{D}n \mathscr{P}(n) A\{n\}$$

$$= \mathscr{N}^{-1} \int \mathscr{D}n \exp[NS\{n\}] A\{n\}, \tag{35}$$

where $\mathscr{N}$ is a normalization constant, and $\mathscr{D}n$ represents a measure on the space of density distributions, concentrated on those which satisfy the ensemble constraints. (We leave aside the subtle problems associated with the rigorous construction of such a measure.) Expanding S in eigenfunctions of the constrained second variation yields

$$\langle A\rangle \approx \int \left[\prod_\nu \left(\frac{-N\lambda_\nu}{2\pi}\right)^{1/2} da_\nu\right] \times \exp\left\{\frac{1}{2} N \sum_\nu a_\nu^2 \lambda_\nu\right\} A\{n_e + \sum_\nu a_\nu n_\nu\}$$

$$\approx A\{n_e\} - \sum_\nu \frac{1}{2N\lambda_\nu} \left(\frac{\partial^2}{\partial x^2} A\{n_e + x n_\nu\}\right)\Big|_{x=0}, \tag{36}$$

where $n_\nu = -\nabla^2 \psi_\nu / 4\pi$. In particular, the dipole variance around symmetric equilibria is approximately

$$\langle D^2\rangle \approx \sum_j \sum_{m=1}^{2} \frac{1}{N|\lambda_{1j}|} \left|\int d^2\mathbf{r}\, \mathbf{r} n_{1jm}\right|^2, \tag{37}$$

where the n_{1jm} for $m = 1,2$ are the $l = 1$ eigenfunctions $\hat{n}_{1j}(r)\cos\theta$ and $\hat{n}_{1j}(r)\sin\theta$. Since the $\hat{n}_{1j}$ are obtained from a Sturm–Liouville problem, the eigenvalues $-\lambda_{1j}$ are ordered by increasing numbers of nodes, which we identify with the index j. As E approaches E_c from below, the principal eigenvalue $\lambda_{10} \propto (E - E_c)$ approaches zero, and $\langle D^2\rangle$ can be approximated by the leading terms

$$\langle D^2\rangle \approx \frac{2\pi^2}{N|\lambda_{10}|} \left(\int dr\, r^2 \hat{n}_{10}\right)^2. \tag{38}$$

In the Gaussian approximation, the variance diverges as $1/(E - E_c)$. Of course, this approximation involves an expansion in small fluctuation amplitudes, so it is inconsistent in the immediate vicinity of the transition. The energy dependence of the dipole variance is shown in Fig. 11. Unfortunately, the poor statistical quality of the Monte Carlo data forbids a quantitative analysis of large fluctuations here. The data does exhibit a large fluctuation level over a broad range of energies around the critical value, consistent with the range of small $|\lambda_{10}|$ shown in Fig. 4.

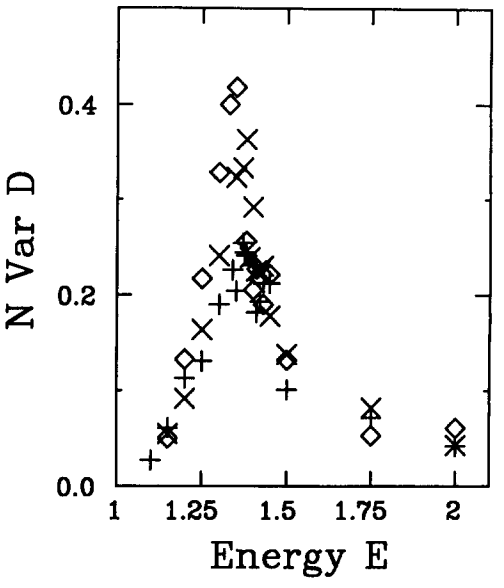

FIG. 11. The dipole variance from the Monte Carlo simulations. A factor of $1/N$ has been removed for comparison of different runs. Symbols as in Fig. 8.

V. THERMODYNAMICS

It may be helpful to summarize the above results by means of a phase diagram. We suppose that the number of rods is fixed, and consider E and M as the independent state variables. Then the state space may be divided into four regions as shown in Fig. 12. Region 1 is bounded by one curve where $\omega = 1$ and another where $\beta = \infty$; it corresponds to the usual axisymmetric equilibria, with density concentrated near the origin. Equilibria in region 2 (similar boundaries, but $M > 0.5$) have significant density near the wall, and are

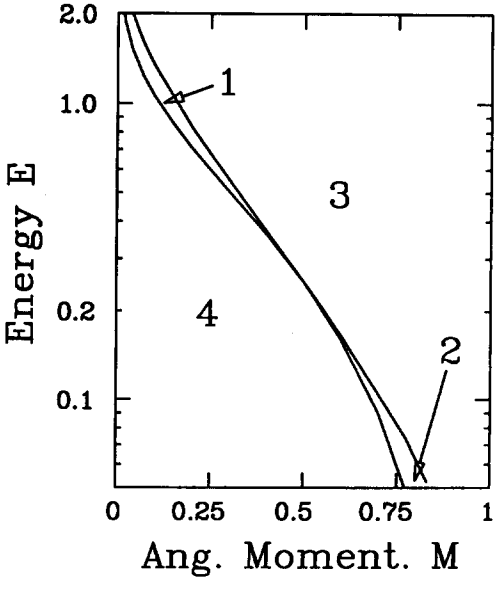

FIG. 12. Phase diagram of the guiding-center system in energy/angular momentum space.

thus unrealizable. Region 3 consists of the displaced equilibria, and region 4 is forbidden because the mean-field energy is not consistent with the specified angular momentum.

It is a simple matter to relate some thermodynamic quantities to the calculations described above. For example, we note that the thermodynamic relation $dS = \beta(dE + \omega\, dM)$ identifies $-\omega$ as the slope of an isentropic path on the E-M plane. By comparison with numerical results for $\omega(E,M)$ (like those shown in Figs. 1–3), these adiabats will have the qualitative form shown in Fig. 13. Furthermore, we can interpret our approximation scheme for large-energy equilibria as the result of a reversible displacement from a symmetric fiducial state A (on the critical curve where $\omega = 1$) to B (at large M) along an adiabat. The approximation that the distribution is not distorted at large D implies that the entropy $-\int d^2\mathrm{r}\, n \ln n$ is nearly identical in the two states (E,M) and (E',M'). The frequency along the curve is found from the force-balance argument, $\omega = 1/(1 - D^2)$, and we integrate to find

$$E - E' = -\int_{M'}^{M} dM\,\omega = -\int_0^D \frac{2D\,dD}{1 - D^2} = \ln(1 - D^2).$$

Another implication of the thermodynamic relation $dS = \beta(dE + \omega\, dM)$ concerns the effect of a small, externally imposed, static asymmetry in the confinement fields. Such asymmetries break the invariance of the Hamiltonian under translations in azimuth, but not under translations in time. Thus they gradually change the angular momentum of the plasma ($dM \neq 0$) but not its energy ($dE = 0$). In response, the plasma evolves through a sequence of states near to thermal equilibrium. For each step in the evolution, the second law implies that $0 \leqslant dS = \beta\omega\, dM$. The state point moves toward larger entropy along a path of constant energy. When the system reaches the entropy maximum along this curve (where $\beta\omega = \partial S/\partial M|_E$), the evolution ceases. Note that the confined states with $\omega = 0$ and $\beta < 0$ (points C in Figs. 1–3) are the states of maximum entropy when the angular momentum constraint is relaxed.

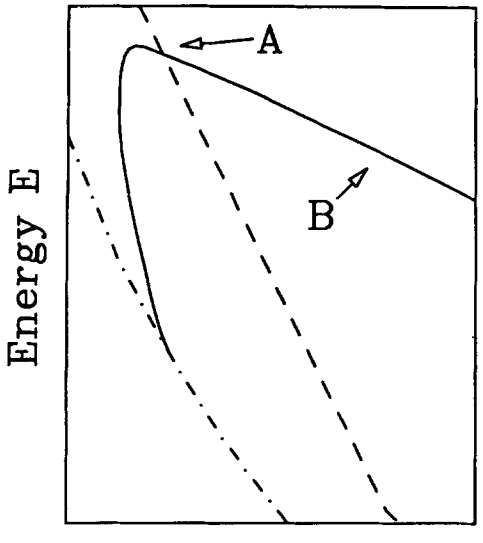

FIG. 13. A representative path of constant entropy (solid line). The dash-dotted line corresponds to $\beta \to \infty$, the dashed line to $\omega = 1$.

A. The canonical ensemble

The circular guiding-center system is unusual in that the canonical and microcanonical ensembles differ qualitatively in certain parameter ranges, even in the large N limit. In a canonical ensemble, where the system is regarded as coupled to a heat bath, beta is specified and the most likely states are those which maximize the total entropy of the system and heat bath. This is usually phrased in terms of the free energy $F = E - S/\beta$, which is minimized for $\beta > 0$ and maximized for $\beta < 0$. In the mean-field approximation, the variational problem for the canonical ensemble leads to the Euler–Lagrange equation treated above, Eq. (5), but the energy constraint is no longer imposed. Furthermore, the stability problem is changed; the second variation of F is taken at fixed β, leading to an eigenvalue problem like Eq. (33), but without $\mathscr{L}_\beta$. In this case, there is a positive eigenvalue for both branches above E_c, as we have verified numerically (by straightforward extension of methods described in Appendix A). From the perspective of bifurcation theory, when β is the bifurcation parameter, the transition at fixed M is a subcritical pitchfork bifurcation. Hence the large energy branches are both unstable; the low-energy, symmetric branch is a local maximum of total entropy, but only a relative maximum of free energy (i.e., a metastable state) for $-2 > \beta > \beta_c$. The distinction arises because the entropy is bounded from above, whereas the free energy is not.

The instability of the off-axis branch is consistent with its negative specific heat at constant M. Suppose the system is weakly coupled to a heat bath at β_B, so that it remains close to a microcanonical equilibrium at each point along a trajectory in the $E\beta$ plane from some initial values β_i, E_i until equilibration at β_B, E_f. The heat transferred to the heat bath is $E_i - E_f$, so the total entropy of the guiding centers plus the heat bath changes by an amount

$$\Delta S = \int_{\beta_i}^{\beta_B} (\beta - \beta_B)\,\frac{\partial E}{\partial \beta}\, d\beta. \tag{39}$$

For the off-axis states, the specific heat $C_M = -\beta^2(\partial E/\partial\beta)$ is negative; the entropy change would violate the second law, so the off-axis states cannot be in equilibrium with a heat bath. If coupled to a heat bath at $\beta < -2$, the guiding-center system would presumably collapse to a single-line vortex.[17] This account is supported by the failure of Monte Carlo simulations of canonical ensembles to converge when $\beta < -2$. (For $\beta > -2$, such simulations appear to be consistent with the microcanonical ones, but the statistics are even poorer.)

VI. DISCUSSION

We may expect the most likely configurations to dominate long-time averages of a typical system, assuming that a generic realization ergodically explores all but a negligible

region of the kinematically accessible phase space. Of course, the degenerate entropy maxima in the large-energy phase all contribute to the long-time average, which would therefore be rotationally symmetric. This is true even in the frame rotating at frequency ω, where fluctuations in the strength of the electric field at the center of charge would lead to slow changes in the azimuthal location of a given realization. This is analogous to the situation in second-order phase transitions; for example, in a vector spin system, there are hydrodynamic spin waves associated with the rotational degeneracy of the ordered phase. (The global nature of the order parameter in this model prevents a precise analogy, since there is nothing to correspond to the wave number of the spin waves.)

There are several limitations to the validity of the two-dimensional guiding-center model as a description of a nonneutral plasma. In practice, of course, the application to experiments must be restricted to cases where the density is negligibly small near the boundary and is everywhere small compared to the Brillouin limit. Since we are invoking a negative effective temperature for the asymmetric configurations, the guiding-center variables are obviously not in equilibrium with the velocity space degrees of freedom of a real plasma. Inclusion of these degrees of freedom would force the temperature to be positive.[22] Hence we expect our description to apply only if there is a separation of time scales such that the statistical equilibration of guiding center positions through $\mathbf{E}\times\mathbf{B}$ flow is rapid compared to exchange of energy with other degrees of freedom; this requires a strong magnetic field. In this case, a separate guiding-center temperature can be defined, and may be negative like the spin temperature of a magnet.[22] The thermal equilibria described here may then characterize such a plasma for intermediate times, before collisional relaxation to the rigid-rotor equilibria of Eq. (3). There is evidence of such time scale separation in recent experiments,[23,24] which indicate evolution dominated by $\mathbf{E}\times\mathbf{B}$ drift dynamics.

Even in the context of 2-D evolution, there are impediments to relaxation. Ideal two-dimensional $\mathbf{E}\times\mathbf{B}$ drift dynamics in the continuum limit preserves all generalized enstrophies, i.e., integrals of the form $\int d^2\mathbf{r}G(n)$, where $n(\mathbf{r},t)$ is the plasma density. (This expresses incompressibility of the nonneutral plasma, which corresponds to the incompressible flow of *vorticity* in an ideal neutral fluid.) The bearing of such constraints on statistical equilibrium models of fluid turbulence has been discussed by Carnevale and Frederiksen.[25] The mean-field entropy is such a functional. For a system of line charges or point vortices, the equilibration process relies on the underlying discreteness, although the mean-field density is continuous. Even in the case of a continuous fluid, we can identify the mean-field distribution with a coarse-grain average, and regard small-scale fluctuations as noise. Rapid mean-field equilibration may then result from violent shear-flow or diocotron instabilities, which lead to fine-scale filamentation of the density. That is, we suppose that segments of a filament behave like discrete rods. The achievement of a point-particle thermal equilibrium in this fashion requires that the turbulence is sufficiently violent to mix the density ergodically, and that coarse-grain average densities are small compared to the peak fine-scale density within a filament. [This assumption can be relaxed by generalizing the statistical description to nonoverlapping fluid elements of finite size.[26,27] This leads to thermal equilibria resembling Fermi distributions, whose low-density limit is equivalent to the Boltzmann distribution of Eq. (2).] Under these rather restrictive conditions, the equilibria which we have described are candidates for the density distributions after violent fluctuations (due to instabilities or vortex merger) have decayed. The experiments described in Ref. 24 are sometimes consistent with these criteria, but not over a wide enough parameter range to allow detailed comparison with the present theory.

It is possible that certain discrete-particle effects of a 3-D plasma can be modeled by a 2-D guiding-center kinetic theory leading to our thermal equilibria. This would be consistent with the $1/B$ scaling of relaxation times observed in a series of quiescent experiments.[28] However, the ergodic hypothesis may be incompatible with experimental conditions. There are many other mean-field dynamical equilibria (where the density is constant along equipotential surfaces, but the relation between n and ϕ differs from the maximum entropy condition). If the time scale for cross-field guiding-center transport is comparable to the scale for exchange of energy with velocity-space degrees of freedom, then the observed guiding-center equilibria may never resemble the maximum entropy ones, but presumably decay to the thermal equilibria of all $3N$ degrees of freedom, which always have positive beta and are axisymmetric. This applies to the experiments described in Ref. 23, for example.

It should be emphasized that the character of the transition depends crucially on the rotational symmetry and the presence of a boundary. If the symmetry of the confinement geometry is broken, the system will drift secularly toward an $\omega = 0$ equilibrium as described in Sec. V, rather than toward some other solution of the problem $n = n_0 \exp[-\beta(\phi + \omega r^2)]$ with different boundary conditions. If the boundary is removed altogether, the equilibria are as described by Lundgren and Pointin,[4] and there are no bifurcations of maximum entropy states. The condition for the transition ($\omega = 1$) is not attained in thermal equilibrium in either of these cases.

ACKNOWLEDGMENTS

This work was supported in part by National Science Foundation Grant No. PHY87-06358 and by Office of Naval Research Contract No. N00014-82-K-0621. Computations were done under an allocation from the San Diego Supercomputer Center.

APPENDIX A: DETAILS OF THE $l=1$ BIFURCATION ANALYSIS

In this appendix, we show that the mean-field equilibria near an $l = 1$ bifurcation off of the symmetric branch at M_0, $E_c(M_0)$ are in correspondence with solutions of the algebra problem

$$x^3 + \{A_1[E - E_c(M_0)] + A_2(M - M_0)\}x = 0, \tag{A1}$$

where x is proportional to the displacement and the constants A_1 and A_2 are determined from the equilibrium at the bifurcation point. The derivation of Eq. (A1) is known as a Lyapunov–Schmidt reduction. The standard methods for elliptic problems (as described in Ref. 29, for example) must be modified to handle the constraints, so the following discussion will be more or less self-contained. We also compute the principal eigenvalue of the second variation of the constrained entropy along the off-axis branch, at leading order in perturbation theory.

Let the increment in the electrostatic potential be expanded as

$$\delta\phi(r,\theta) = x\psi(r,\theta) + f^{(2)}(r,\theta) + f^{(3)}(r,\theta) + \cdots, \tag{A2}$$

where $f^{(j)} = \mathcal{O}(x^j)$. We proceed by substituting Eq. (A2) into

$$n + \delta n = \exp[-(\beta + \delta\beta)(\phi + \delta\phi) - (\alpha + \delta\alpha)r^2 - \gamma - \delta\gamma] \tag{A3}$$

and the constraints. (For the remainder of this section, terms without δ are considered fixed at their bifurcation values.) Without loss of generality we can take $\psi = \hat{\psi}(r)\cos\theta$. This identifies the null solution of Eq. (A1) with the symmetric branch of equilibria, and the nontrivial solutions with the displaced branch. At $\mathcal{O}(x)$, we obtain $\mathcal{L}_1\hat{\psi} = 0$; the solution is discussed in Sec. II. At $\mathcal{O}(x^2)$ we obtain the linear system

$$Lf^{(2)} = 4\pi n(-\tfrac{1}{2}\beta^2 x^2\psi^2 + r^2\delta\alpha + \phi\delta\beta + \delta\gamma), \tag{A4a}$$

$$0 = \int d^2\mathbf{r}\,\nabla^2 f^{(2)} = -\int d\theta \left.\frac{\partial f^{(2)}}{\partial r}\right|_{r=1}, \tag{A4b}$$

$$\delta M = -\frac{1}{\pi}\int d^2\mathbf{r}\, f^{(2)}, \tag{A4c}$$

and

$$\delta E = \int d^2\mathbf{r}\, n f^{(2)} - \frac{1}{2}x^2\pi\beta\int d^2\mathbf{r}\, n\psi^2, \tag{A4d}$$

where $L = (\nabla^2 - 4\pi n\beta)$. The right-hand side of Eq. (A4a) includes azimuthal modes $l = 0$ and 2. Generically, L is nonsingular except for $l = 1$, so the Fredholm solubility condition—that the right-hand side be orthogonal to the singular eigenfunction ψ of L—is trivial. Hence we can express $f^{(2)}$ in terms of $\delta\alpha$, $\delta\beta$, and $\delta\gamma$ by integrating Eq. (A4a). At third order

$$Lf^{(3)} = 4\pi n x\psi(\delta\beta - \beta^2 f^{(2)} - \beta r^2\delta\alpha - \beta\phi\,\delta\beta - \beta\,\delta\gamma + x^2\tfrac{1}{8}\beta^3\psi^2) + \text{terms independent of } \theta. \tag{A5}$$

The value of x consistent with prescribed δE and δM is determined from the solubility condition at this order:

$$0 = x\int d^2\mathbf{r}\, n\psi^2(\beta^2 f^{(2)} + \beta r^2\,\delta\alpha + \beta\phi\,\delta\beta + \beta\,\delta\gamma + \delta\beta) + \frac{1}{6}x^3\int d^2\mathbf{r}\, n\psi^4. \tag{A6}$$

It is convenient to introduce the functions $\chi_j(r)$ defined by

$$\begin{aligned}
\left(\frac{1}{r}\frac{d}{dr}r\frac{d}{dr} - 4\pi\beta n\right)\chi_1 &= 4\pi n r^2,\\
\left(\frac{1}{r}\frac{d}{dr}r\frac{d}{dr} - 4\pi\beta n\right)\chi_2 &= 4\pi n\phi,\\
\left(\frac{1}{r}\frac{d}{dr}r\frac{d}{dr} - 4\pi\beta n\right)\chi_3 &= 4\pi n,\\
\left(\frac{1}{r}\frac{d}{dr}r\frac{d}{dr} - 4\pi\beta n\right)\chi_4 &= 4\pi n\hat{\psi}^2,\\
\left(\frac{1}{r}\frac{d}{dr}r\frac{d}{dr} - \frac{4}{r^2} - 4\pi\beta n\right)\chi_5 &= 4\pi n\hat{\psi}^2,
\end{aligned} \tag{A7}$$

with χ_j regular at $r = 0$ and vanishing at $r = 1$, and the normalization constant $I = \int dr\, r n\hat{\psi}^2$. Then the constraints and the solubility condition can be written as

$$\mathbf{Q}\begin{pmatrix}\delta\alpha\\ \delta\beta\\ \delta\gamma\\ x^2/4\end{pmatrix} = \begin{pmatrix}-2\delta N\\ -\tfrac{1}{2}(\delta M - \delta N)\\ \beta\,\delta E/\pi\\ 0\end{pmatrix} = \begin{pmatrix}0\\ -\tfrac{1}{2}\delta M\\ \beta\delta E/\pi\\ 0\end{pmatrix}, \tag{A8}$$

where the elements of the matrix $\mathbf{Q}$ are given by

$$\begin{aligned}
Q_{1j} &= \chi_j'(1) \quad j = 1,\ldots,4,\\
Q_{2j} &= \int dr\, r\chi_j \quad j = 1,\ldots,4,\\
Q_{3j} &= \int dr\, nr\chi_j \quad j = 1,2,3,\\
Q_{34} &= \int dr\, nr\chi_4 + 4\int dr\, rn\hat{\psi}^2,\\
Q_{41} &= \int dr\, rn\hat{\psi}^2(r^2 + \chi_1),\\
Q_{42} &= \int dr\, rn\hat{\psi}^2(\phi - \beta^{-1} + \chi_2),\\
Q_{43} &= \int dr\, rn\hat{\psi}^2(1 + \chi_3),\\
Q_{44} &= \int dr\, rn\hat{\psi}^2\left(\chi_4 + \frac{1}{2}\chi_5 + \frac{1}{2}\hat{\psi}^2\right).
\end{aligned} \tag{A9}$$

From Eq. (A8), it is clear that the entries in the matrix inverse of $\mathbf{Q}$ are simply related to thermodynamic derivatives like $\partial\beta/\partial E$ at the transition point. Given an equilibrium satisfying the criterion for bifurcation ($\omega = 1$), the χ_j and the elements of $\mathbf{Q}$ can be obtained by numerical integration of Eqs. (A7) and (A9); $\mathbf{Q}$ can then be inverted numerically. Such computations for $M = 0.1$ were used to construct the dashed curves in Figs. 1–3 and 10. In particular, they indicate that the bifurcation is a forward pitchfork with respect to δE when $\delta M = 0$.

1. Perturbation theory for the principal eigenvalue

The same approach can be used to evaluate the leading nontrivial eigenvalue of $\delta^2 S/\delta n^2$ along the off-axis branch at order δE. We consider an equilibrium at a finite displacement amplitude x away from the bifurcation point. Thus the equilibrium quantities n, β, and ϕ are expanded in powers of x: for instance, $n = \Sigma_j n^{(j)}(r,\theta)$, where $n^{(j)} \propto x^j$, and $n^{(0)}$ is the density at the transition. We write the eigenvalue problem, Eq. (33), as

$$[\nabla^2 - 4\pi n(\beta+\lambda)]\psi = 4\pi\beta^{(0)} n(r^2 a + \phi b + c). \quad \text{(A10)}$$

The functionals $\mathscr{L}_\alpha$, $\mathscr{L}_\beta$, and $\mathscr{L}_\gamma$, which are evaluated at ψ, are represented by the constants a, b, and c; these will be determined from the constraints. (The factor of $\beta^{(0)}$ simplifies later notation.) The terms a, b, c, ψ, and λ in Eq. (A10) are also expanded in orders of the displacement amplitude x: $a = \Sigma_{j=1} a^{(j)}$, etc. The leading order change in the equilibrium potential, $\phi^{(1)}$, is just $x\psi^{(0)}$, which we again take proportional to $\cos\theta$. The operators in the perturbed problem are still invariant under the parity operation $\theta \to -\theta$, so eigenfunctions are even or odd. The principal odd eigenfunction is the rotation $\partial\phi/\partial\theta$ (with zero eigenvalue); the principal even eigenfunction can be expanded in cosine harmonics. At $\mathscr{O}(x)$ we encounter the regular problem

$$L^{(0)}\psi^{(1)} = 4\pi\beta^{(0)}[n^{(1)}\psi^{(0)} + n^{(0)}(a^{(1)}r^2 + b^{(1)}\phi^{(0)} + c^{(1)})], \quad \text{(A11)}$$

since $\lambda^{(1)}$ vanishes by symmetry. At $\mathscr{O}(x^2)$, there is a solubility condition

$$0 = \int d^2\mathbf{r}\,\psi^{(0)} L^{(0)}\psi^{(2)} \propto \int d^2\mathbf{r}\,\psi^{(0)}\left[n^{(1)}\psi^{(1)} + n^{(2)}\psi^{(0)} + \left(\frac{\lambda^{(2)}+\beta^{(2)}}{\beta^{(0)}}\right)n^{(0)}\psi^{(0)} + n^{(1)}(a^{(1)}r^2 + b^{(1)}\phi^{(0)} + c^{(1)}) + n^{(0)}b^{(1)}\phi^{(1)}\right]. \quad \text{(A12)}$$

(Terms such as the one involving $a^{(2)}$ are annihilated by integration over θ.) The first-order constraints are equivalent to

$$0 = \int d^2\mathbf{r}\,\nabla^2(\psi^{(0)} + \psi^{(1)}) \propto \int d\theta \left.\frac{d\psi^{(1)}}{dr}\right|_{r=1},$$
$$0 = \int d^2\mathbf{r}(\psi^{(0)} + \psi^{(1)}) \propto \int d^2\mathbf{r}\,\psi^{(1)}, \quad \text{(A13)}$$
$$0 = \int d^2\mathbf{r}(n^{(0)}\psi^{(1)} + \psi^{(0)}n^{(1)}) = \int d^2\mathbf{r}\,n^{(0)}[\psi^{(1)} - \beta^{(0)}(\psi^{(0)})^2].$$

After substituting for the equilibrium terms computed in the course of the bifurcation analysis, the constraints and the solubility condition reduce to

$$\frac{\lambda^{(2)}}{\beta^{(0)}}\int dr\, r n^{(0)}\hat{\psi}^2\begin{pmatrix}0\\0\\0\\1\end{pmatrix} = x\mathbf{Q}\begin{pmatrix}a^{(1)}\\b^{(1)}\\c^{(1)}\\-x/2\end{pmatrix}. \quad \text{(A14)}$$

This is a linear algebra problem whose solution yields the constant of proportionality between $\lambda^{(2)}$ and x^2 (as well as the coefficients in the perturbed eigenfunction, $a^{(1)}$, $b^{(1)}$, and $c^{(1)}$). Finally the perturbed eigenvalue at energy E is obtained by expressing x^2 in terms of the energy increment to second order:

$$\lambda \sim \lambda^{(2)} = \frac{\lambda^{(2)}}{x^2}x^2 \sim \frac{\lambda^{(2)}}{x^2}(E - E_c)\left.\frac{\partial(x^2)}{\partial E}\right|_{E=E_c}, \quad \text{(A15)}$$

where the last derivative is obtained from $\mathbf{Q}^{-1}$. The numerical solution of this system yielded the results shown in Fig. 4(b).

APPENDIX B: EIGENVALUES FOR SYMMETRIC PERTURBATIONS

In the text, we used the fact that there are no symmetric singularities of the second variation operator $\delta^2 S/\delta n^2$ which might lead to positive eigenvalues for the equilibria of interest. That is, all symmetric singularities occur at thermodynamically irrelevant values of beta. (They typically occur on secondary symmetric branches, at energies larger than the critical energy for the $l = 1$ bifurcation.)

This picture is consistent with our numerical evaluation of eigenvalues of the second variation. We can write the eigenvalue problem as

$$\nabla^2\psi - 4\pi n(\beta+\lambda)\psi = 4\pi n(a_1 r^2 + a_2\phi + a_3),$$

where the coefficients a_j are determined from the first-order constraints. This computation is rather delicate, because of the sensitivity of eigenvalues for the fully constrained problem. We found the following method for obtaining these eigenvalues to be fairly robust. We integrate Eq. (A7), with beta replaced by $\beta + \lambda$, for $j = 1,2,3$. Now the solution ψ is a linear combination $\Sigma_j a_j\chi_j$. The constraints form a singular linear algebra problem for the a_j. Hence an eigenvalue is a value of λ such that this linear algebra problem has a vanishing determinant. Such values of λ are located by a numerical root finder; the algorithm is thus a generalized shooting scheme. This method was used to construct the curve in Fig. 4, and checked against unphysical singularities of the equilibrium problem, which were obtained independently as unfoldings of a degenerate bifurcation (whose details need not concern us here).

APPENDIX C: COMPUTING OFF-AXIS MEAN-FIELD EQUILIBRIA

Numerical approximations to solutions of Eq. (5) were obtained by use of a conjugate-gradient-continuation scheme, closely following the algorithm of Glowinski, Keller, and Reinhart.[30] (Simpler methods were not found to be as robust.) First we introduce a more convenient normalization for the numerical work; let $u(r,\theta) = \ln[n(r,\theta)/n(1)]$. Then we are looking for solutions to the generalized Bratu problem

$$\nabla^2 u - \lambda e^u + 4\alpha = 0, \quad u(1,\theta) = 0, \quad \text{(C1)}$$

where α and λ are easily related to β and ω by normalizing after the solution has been obtained. We impose the angular

momentum constraint in the form $\int d^2\mathbf{r}\, e^u(r^2 - M) = 0$, and augment the system with a continuation formula

$$\int d^2\mathbf{r}\, \nabla\dot{u}_0\cdot\nabla(u - u_n) + \dot{\lambda}_0(\lambda - \lambda_n) + \dot{\alpha}_0(\alpha - \alpha_n) = \Delta s,$$

where s is a pseudoarclength, the dot indicates a derivative with respect to s, and $(u_n, \lambda_n, \alpha_n)$ is a reference solution. To obtain the asymmetric branch, we start at the bifurcation point $(u_0, \lambda_0, \alpha_0)$, where we can approximate the initial tangent $(\dot{u}_0, \dot{\lambda}_0, \dot{\alpha}_0)$ from the analytical results in Sec. II. (Subsequently, we use a finite difference approximation to the tangent.) We approximate the positive-definite quadratic form

$$J(u,\lambda,\alpha) = \frac{1}{2}\int d^2\mathbf{r}|\nabla\xi|^2 + \frac{\mu^2}{2} + \frac{\nu^2}{2}, \tag{C2}$$

where

$$\xi = u - \lambda\nabla^{-2}e^u + \alpha(r^2 - 1),$$

$$\mu = \int d^2\mathbf{r}[\nabla\dot{u}_n\cdot\nabla(u - u_n) + \dot{\lambda}_n(\lambda - \lambda_n) + \dot{\alpha}_n(\alpha - \alpha_n)] - \Delta s,$$

$$\nu = \int d^2\mathbf{r}\, e^u(r^2 - M),$$

by representing u in terms of finite elements in r and Fourier components in θ. Then a conjugate-gradient algorithm is used to minimize J, starting at the result of an Euler predictor, $u_n + \dot{u}_n\Delta s$. The gradient calculations involve extensive use of a fast cylindrical Poisson solver. The algorithm is iterated to construct the solution branch parametrized by the arclength s. It appears to be more robust than schemes used by others for similar problems,[31,32] and is simpler than methods based on full Newton iteration.

[1] R. A. Smith, Phys. Rev. Lett. **63,** 1479 (1989).
[2] D. Montgomery and R. H. Kraichnan, Rep. Prog. Phys. **43,** 547 (1980).
[3] S. Kida, J. Phys. Soc. Jpn. **39,** 1395 (1975).
[4] T. S. Lundgren and Y. B. Pointin, J. Stat. Phys. **17,** 323 (1977).
[5] J. H. Williamson, J. Plasma Phys. **17,** 85 (1977).
[6] R. C. Davidson and N. Krall, Phys. Rev. Lett. **22,** 833 (1969); R. C. Davidson and N. Krall, Phys. Fluids **13,** 1543 (1970).
[7] T. M. O'Neil and C. F. Driscoll, Phys. Fluids **22,** 266 (1979).
[8] L. Onsager, Nuovo Cimento, Suppl. **6,** 279(1949).
[9] G. Joyce and D. Montgomery, J. Plasma Phys. **10,** 107 (1973).
[10] S. F. Edwards and J. B. Taylor, Proc. R. Soc. London, Ser. A **336,** 257 (1974).
[11] D. Montgomery and G. Joyce, Phys. Fluids **17,** 1139 (1974).
[12] C. E. Seyler, Jr., Phys. Fluids **19,** 1336 (1976).
[13] Y. B. Pointin and T. S. Lundgren, Phys. Fluids **19,** 1459 (1976).
[14] T. S. Lundgren and Y. B. Pointin, Phys. Fluids **20,** 356 (1977).
[15] J. H. Malmberg and T. M. O'Neil, Phys. Rev. Lett. **39,** 1333 (1977).
[16] R. H. Levy, Phys. Fluids **8,** 1288 (1965).
[17] R. H. Kraichnan, J. Fluid Mech. **67,** 155 (1975); see also A. M. Saltzberg, J. Math. Phys. **6,** 158 (1965).
[18] V. I. Arnol'd, J. Méc. **5,** 29 (1966).
[19] D. D. Holm, J. E. Marsden, T. Ratiu, and A. Weinstein, Phys. Rep. **123,** 1 (1985).
[20] M. Creutz, Phys. Rev. Lett. **50,** 1411 (1983).
[21] D. Stauffer and A. L. Fetter, Phys. Rev. **168,** 156 (1968).
[22] L. D. Landau and E. M. Lifshitz, *Statistical Physics* (Pergamon, London, 1980), 3rd ed.
[23] K. S. Fine, C. F. Driscoll, and J. H. Malmberg, Phys. Rev. Lett. **63,** 2232 (1989).
[24] C. F. Driscoll and K. S. Fine, Phys. Fluids B **2,** 1359 (1990).
[25] G. F. Carnevale and J. S. Frederiksen, J. Fluid Mech. **175,** 157 (1987).
[26] D. Lynden-Bell, Mon. Not. R. Astron. Soc. **136,** 101 (1967).
[27] J. Miller, Phys. Rev. Lett. (in press).
[28] C. F. Driscoll, J. H. Malmberg, and K. S. Fine, Phys. Rev. Lett. **60,** 1290 (1988).
[29] M. Golubitsky and D. Schaeffer, *Singularities and Groups in Bifurcation Theory* (Springer, Berlin, 1986).
[30] R. Glowinski, H. B. Keller, and L. Reinhart, SIAM J. Sci. Stat. Comput. **6,** 793 (1985).
[31] B. E. McDonald, J. Comput. Phys. **16,** 360 (1974); D. L. Book, S. Fisher, and B. E. McDonald, Phys. Rev. Lett. **34,** 4 (1975).
[32] B. Marder and H. Weitzner, J. Plasma Phys. **12,** 435 (1970).